Experimental study of the reversible behavior of modulational instability in optical fibers

Gaetan Van Simaeys, Philippe Emplit, and Marc Haelterman

Service d'Optique et d'Acoustique, Université Libre de Bruxelles, 50 Avenue F. D. Roosevelt, C.P. 194/5, B-1050 Brussels, Belgium

Received May 22, 2001; revised manuscript received September 6, 2001

We report what is to our knowledge the first clear-cut experimental evidence of the reversibility of modulational instability in dispersive Kerr media. It was possible to perform this experiment with standard telecommunication fiber because we used a specially designed 550-ps square-pulse laser source based on the two-wavelength configuration of a nonlinear optical loop mirror. Our observations demonstrate that reversibility is due to well-balanced and synchronous energy transfer among a significant number of spectral wave components. These results provide what we believe is the first evidence, in the field of nonlinear optics, of the universal Fermi–Pasta–Ulam recurrence phenomenon that has been predicted for a large number of conservative nonlinear systems, including those described by a nonlinear Schrödinger equation that is relevant to the context of the present study. © 2002 Optical Society of America

OCIS codes: 190.3100, 190.4380, 190.4370, 060.4370.

1. INTRODUCTION

Modulational instability (MI) refers to the phenomenon in which an initially perturbed continuous wave (cw) tends to break up spontaneously into a periodic solitonlike pulse train while it propagates through a nonlinear dispersive medium such as an optical fiber. In the frequency domain, this phenomenon can be interpreted as a phase-matched partially degenerate four-wave mixing process in which an intense pump wave yields energy to a pair of weak sideband waves, i.e., a Stokes (redshifted) and an anti-Stokes (blueshifted) sideband wave, symmetrically located on the two sides of the pump wave. In this paper we consider only the scalar MI process that does not involve alteration of the polarization state of light. In this case the required phase-matching condition can be obtained only with negative (anomalous) group-velocity dispersion because of the positive nonlinear index coefficient of silica, the constituent of the optical fibers that we have chosen to use as a nonlinear material in our experiment.

From a mathematical point of view, the scalar MI in optics is formally equivalent to the so-called Benjamin–Feir instability predicted in the context of hydrodynamics through a linear stability analysis.[1,2] The Benjamin–Feir approach applied to the nonlinear Schrödinger (NLS) equation that is relevant to the present study allows one to predict the conditions of occurrence of MI as well as the initial growth rate and the characteristic frequency of the instability. However, because this approach relies on perturbative analysis, it does not yield information about the long-term behavior of a modulationally unstable wave. The initial exponential growth of the weak spectral sideband pair predicted by linear stability analysis obviously occurs at the expense of the pump wave. Once the pump wave is significantly depleted, growth of the sidebands is no longer exponential, and a more-complex energy transfer process takes place in the system. The dynamics of MI in the pump-depletion regime was described by Lake *et al.*[3] and by Yuen and Ferguson[4] in the framework of their study of nonlinear deep-water waves in which they demonstrated, in particular, that the NLS equation reproduces the Benjamin–Feir instability. By means of numerical simulations of the NLS equation with a perturbed uniform wave as an initial condition, they showed that, after the initial exponential growth predicted by Benjamin and Feir, the modulation amplitude reaches a maximum and then decreases until the system eventually returns to (near) its initial state, in this way showing that MI is reversible. This process of growth and decay proceeds almost periodically, at least for the first few characteristic periods. Correspondingly, the energy of the wave initially confined to the carrier frequency (or fundamental) mode periodically experiences a spreading to a few neighboring sideband modes followed by an almost complete return to the initial condition, as illustrated in Fig. 1. This time-periodic return of the solution to the nearly unmodulated initial state is known as the *Fermi–Pasta–Ulam* (FPU) *recurrence* phenomenon.[5] FPU recurrence was reported for the first time to our knowledge by Fermi *et al.*[5] in the framework of a numerical study of one-dimensional vibrating chains of equimass particles connected by linear and weakly nonlinear springs. They expected that the nonlinear coupling between neighboring oscillating masses, which is responsible for energy exchange between the vibration modes, would eventually lead to an irreversible equipartition of energy over a broad spectrum, i.e., that the system would "thermalize."[5] Instead, they observed a seemingly periodic exchange of energy among only a few higher-order modes and the fundamental mode, where the energy was initially confined. Almost all the energy returned to the

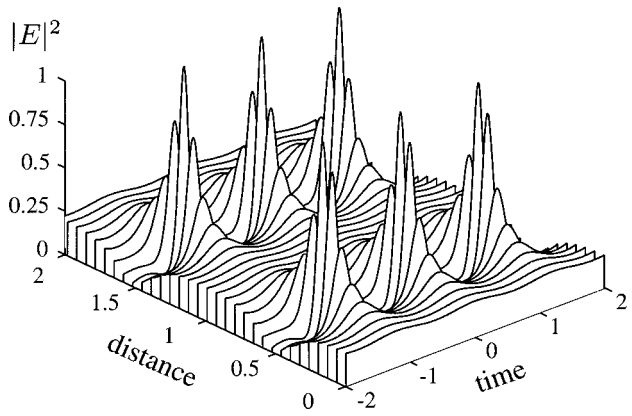

Fig. 1. Spatiotemporal evolution of MI. (The parameters used here for the simulation are those given in Subsection 2.B for an input pump power of 2 W.)

initially excited mode after a time known as the FPU recurrence time. FPU recurrence is ubiquitous in nonlinear science, as revealed by the large variety of research fields, such as plasma physics[6,7] and hydrodynamics,[1] in which it has been theoretically predicted.

In nonlinear fiber optics, much attention has been devoted to the theoretical study of MI dynamics. In particular, the pump-depletion regime was conveniently analyzed through the so-called truncated three-mode approximation that reduces the NLS equation to a set of coupled ordinary differential equations that describe the nonlinear interaction between the pump wave, at carrier frequency ω_0, and the first two contiguous sideband waves, at frequencies $\omega_0 \pm \Omega$.[8–10] It has been shown that, if the sideband detuning from the pump Ω satisfies the phase-matching condition required for MI, the higher-order Fourier modes can be neglected in a good approximation, as they fall outside the MI gain band.[8,11] By means of an analysis based on invariant quantities of the problem, it has been shown[10] that the entire dynamics of the MI process can be depicted by means of a one-dimensional conservative Hamiltonian. The recurrent (i.e., periodic) evolution of the waves is then represented as closed trajectories in the phase-space portrait of this Hamiltonian. This representation provides an intuitive insight into the dynamics of the system and permits direct interpretation of the complex nonlinear behavior of MI. For instance, this approach easily shows that, depending on the parameters of the system and the initial amplitudes and phases of the three waves, the evolution may or may not be spatially periodic.

Nevertheless, as the higher-order modes are neglected in this approach, the model is not complete and, in particular, cannot take into account the energy spreading to the higher-order modes that is characteristic of the FPU recurrence phenomenon.[3–5] In response to this difficulty, Akhmediev and co-workers developed another approach to the problem.[12,13] They derived exact analytical spatiotemporal periodic solutions to the NLS equation (in terms of Jacobi elliptic functions) that represent the spatial evolution of initially continuous (or periodically modulated) waves. As a consequence, their approach inherently accounts for an arbitrary number of interacting sideband modes. In this way, Akhmediev *et al.* have been able to predict that in the MI process the energy will be spectrally distributed among the higher-order modes according to a geometric progression law; i.e., the logarithm of the energy of the higher-order modes will decrease linearly with the mode order.[12] This finding has been confirmed by computer simulations of the NLS equation.

This extensive theoretical study has yielded a complete picture of the dynamics of a modulationally unstable wave in a single-mode optical fiber, from the onset of MI to the long-term evolution beyond the early stage of the undepleted pump. However, numerous experiments with MI have focused mainly on the first stage of modulation growth. To our knowledge, in only one paper[14] has long-term nonlinear evolution of MI in silica optical fibers been reported. That paper dealt with polarization MI in normally dispersive weakly birefringent fibers. Although nonmonotonic pump and sideband power evolution was observed, the experiments did not provide clear evidence of the reversibility (or FPU recurrence) of the process because of the rather low Raman power threshold of these fibers.[14] As a matter of fact, until now the only experimental proof of which we are aware of the recurrent behavior of MI in a system governed by the NLS equation was provided in 1977 in the field of hydrodynamics in the paper by Lake *et al.* mentioned above.[3] The present study fills this gap in nonlinear optics and experimentally demonstrates, for the first time to our knowledge, the theoretically predicted reversible behavior of MI in a single-mode silica optical fiber. As we shall see, the experimental observations prove to be in excellent agreement with theoretical predictions.

The remainder of the paper is organized as follows. In Section 2 we present the theory of MI in the strong-conversion regime in the presence of Raman scattering and linear attenuation. We also discuss the effects of localized loss on sideband evolution because, as we shall see below, such a loss corresponds to our experimental conditions when a coupler is inserted into the propagation fiber to substantiate our interpretation of the experimental observations. In Section 3 we describe the pump laser source that we used in our experiment. This source is based on a nonlinear loop mirror in a two-wavelength configuration. It is unique in the sense that it generates square-shaped pulses that constitute the keystone of our demonstration of MI reversibility in optics. In Section 4 we describe the experimental procedure and compare our observations with the theoretical predictions presented in Subsection 2.B. Particular attention is devoted to a comparison of our observations and the predictions of the truncated three-wave model. Finally, we present our conclusions in Section 5.

2. THEORY

A. Theoretical Models

In this section we review the most relevant theories that deal with MI in optical waves with the aim of gaining physical insight into the nonlinear dynamics that we observe in our experiment. We thus focus on the dynamicfeatures that we believe are experimentally evidenced for the first time in fiber optics.

As a starting point, we consider the NLS equation that governs the propagation of wave envelopes in optical fibers:

$$\frac{\partial E}{\partial z} = -i\beta_2 \frac{\partial^2 E}{\partial t^2} + i\gamma |E|^2 E, \tag{1}$$

where E is the electric field envelope, z is the propagation distance, t is the time in a reference frame traveling at the group velocity of light, β_2 is the dispersion coefficient, and $\gamma = 2\pi n_2/\lambda A_{\text{eff}}$ is the nonlinear coefficient, where λ is the wavelength of light, A_{eff} is the effective core area of the fiber, and n_2 is the nonlinear index coefficient. To derive the basic characteristics of MI one usually resorts to a linear stability analysis of the perturbed cw solution to Eq. (1), namely, $E(t,z) = [\sqrt{P_0} + a(t,z)]\exp(i\gamma P_0 z)$, where P_0 is assumed constant and with $|a|^2 \ll P_0$. Linearizing with respect to a, one gets the following dispersion relation:

$$K = \pm 1/2|\beta_2|\Omega[-\Omega^2 - \text{sgn}(\beta_2)\Omega_c^2]^{1/2}, \tag{2}$$

where K and Ω, respectively, are the gain and the frequency of the MI, as defined by $a(t,z) \propto \exp(Kz)\cos(\Omega t)$. From Eq. (2) one can easily deduce that K exhibits a positive real part (corresponding to the onset of the instability) only in the anomalous-dispersion regime ($\beta_2 < 0$) and that the MI spectral gain curve, $\text{Re}[K(\Omega)]$, peaks at the value $K = \gamma P_0$ for $\Omega = (2\gamma P_0/|\beta_2|)^{1/2} = \Omega_{\text{opt}}$ and exhibits a finite bandwidth that is bounded by $\Omega_c = \sqrt{2}\Omega_{\text{opt}}$. It turns out that the value $|\Omega| = \Omega_{\text{opt}}$ corresponds to the phase-matching condition of the underlying four-wave mixing interaction between the carrier wave at frequency ω_0 and the first two contiguous modulational sidebands at frequencies $\omega_0 \pm \Omega$. It is easy to show that this phase matching occurs whenever the linear contribution to the wave-vector mismatch that is due to group-velocity dispersion, $\Delta k = \beta_2\Omega^2$, is exactly compensated for by the nonlinear contribution, $\Delta k_{\text{NL}} = 2\gamma P_0$, such that $\Delta k = -\Delta k_{\text{NL}}$.

The most convenient technique for going beyond the limit of validity of this linear stability analysis with which to describe the depleted-pump regime and obtain information about the long-term MI behavior relies on a truncated three-wave model.[8–11] In this approach the phenomenology of MI is limited to the interaction between the pump wave and the pair of Stokes and anti-Stokes waves of frequencies $\omega_s = \omega_0 - \Omega$ and $\omega_a = \omega_0 + \Omega$, respectively. Provided that the sideband detuning from the cw pump Ω satisfies $\Omega_c/2 < |\Omega| < \Omega_c$, the higher-order Fourier modes may be neglected, as they fall outside the MI gain band and are therefore not linearly unstable. In the analysis given in Refs. 10 and 15, it is shown that the evolution of the system is then governed by the following set of three coupled-mode ordinary differential equations:

$$-i\frac{dE_0}{dz} = \gamma[|E_0|^2 + 2(|E_s| + |E_a|)]E_0 + 2\gamma E_s E_a E_0^* \exp(+i\Delta k z), \tag{3a}$$

$$-i\frac{dE_s}{dz} = \gamma[|E_s|^2 + 2(|E_a| + |E_0|)]E_s + 2\gamma E_a^* E_0^2 \exp(-i\Delta k z), \tag{3b}$$

$$-i\frac{dE_a}{dz} = \gamma[|E_a|^2 + 2(|E_s| + |E_0|)]E_a + 2\gamma E_s^* E_0^2 \exp(-i\Delta k z), \tag{3c}$$

where $E_0(z)$ is the pump amplitude, $E_s(z)$ and $E_a(z)$ are the Stokes and anti-Stokes waves, respectively, and $\Delta k = k_s + k_a - 2k_0$ is the linear wave-vector mismatch. Note that the last coherent terms on the right-hand sides of Eqs. (3) are responsible for energy exchanges between the waves. Other cubic terms that represent the generation of new frequency components have been neglected, as they are not phase matched. Accordingly, one can easily verify from Eqs. (3) that the total power $P_{\text{tot}} = |E_0|^2 + |E_a|^2 + |E_s|^2$ is conserved. Equations (3) are then conveniently rewritten in terms of the amplitude and the phase of the three waves as defined through the relations $E_j = |E_j|\exp(i\Phi_j) = A_j \exp(i\Phi_j)$, with $j = 0, a, s$. Introducing the normalized pump power $\eta(z) \equiv A_0^2(z)/(P_{\text{tot}})^{1/2}$, the normalized sideband amplitudes $a_a(z) \equiv A_a(z)/(P_{\text{tot}})^{1/2}$ and $a_s \equiv A_s(z)/(P_{\text{tot}})^{1/2}$, and the scaled longitudinal coordinate $\xi = \gamma P_{\text{tot}} z$, we can recast the system of Eqs. (3) into four equivalent real equations:

$$\frac{d\eta}{d\xi} = -4\eta a_s a_a \sin\Phi, \tag{4a}$$

$$\frac{da_s}{d\xi} = \eta a_a \sin\Phi, \tag{4b}$$

$$\frac{da_a}{d\xi} = \eta a_s \sin\Phi, \tag{4c}$$

$$\frac{d\Phi}{d\xi} = \kappa + [2\eta - (a_s^2 + a_a^2)]\sin\Phi + \left[\eta\left(\frac{a_s}{a_a} + \frac{a_a}{a_s}\right) - 4a_s a_a\right]\cos\Phi, \tag{4d}$$

where $\Phi(\xi) = \kappa\xi + \Phi_a(\xi) + \Phi_s(\xi) - 2\Phi_0(\xi)$ is the phase that governs the four-wave mixing process and $\kappa = \beta_2\Omega^2/\gamma P_{\text{tot}}$ is the normalized linear wave-vector mismatch. Equations (4) provide some physical interpretation of the three-wave approximate model [Eqs. (3)]. Indeed, the last equation of Eqs. (4) reveals that the power flow between the pump and the sidebands depends only on their relative phase. When $\sin\Phi > 0$, power flows from the pump to the sidebands, whereas the reverse occurs when $\sin\Phi < 0$. Maximum power transfer is obtained for $\Phi = \pm\pi/2$. In particular, if we consider an in-

tense pump wave propagating with two weak sidebands (i.e., $a_s^2 + a_a^2 \ll \eta \approx 1$), we find from Eq. (4d) that the sideband growth rate reaches a maximum for $\kappa = -2$, or, equivalently, for $|\Omega| = (2\gamma P_{\mathrm{tot}}/|\beta_2|)^{1/2}$, which is nothing but the detuning that corresponds to maximum MI gain, Ω_{opt}, found in the linear stability analysis.

We can pursue the analysis of the system dynamics further by reducing the whole set of Eqs. (4) to a single equation for the normalized pump power η by means of three invariant quantities of the problem.[8,9] Solutions for this equation may be found in terms of Jacobi elliptic functions. For suitable initial conditions, these solutions exhibit FPU recurrence, and the calculated recurrence distance compares well with that obtained in numerical simulations of Eq. (1).

Resorting to the same three invariants, Cappellini and Trillo showed[10] that the entire dynamics of model equations (4) can be conveniently described by means of a one-dimensional conservative Hamiltonian whose canonical conjugate variables are pump power η and phase Φ. The recurrent evolution of the waves is then depicted by closed trajectories in the phase-space portrait of this Hamiltonian in polar coordinates (η, Φ). Besides the appealing intuitive description that it permits, this model accurately predicts the recurrence distances and provides a clear insight into the long-term behavior of MI (see also Refs. 14–16).

Finally, Akhmediev and co-workers[12,13] have obtained, by means of direct substitution, exact solutions of the NLS equation for an initial modulationally unstable pump cw perturbed by two small Stokes and anti-Stokes sidebands symmetrically located about the pump frequency. They expressed the solution in the form of the Fourier expansion

$$u(z,t) = f_0(z) + 2\sum_{n=1}^{\infty} f_n(z)\cos[n(t - t_0)\sqrt{2}]. \quad (5)$$

They found that the system exhibits a recurrent behavior and that the energy contained in the higher harmonics $|f_n(z)|^2$ decreases according to a geometric progression for any value of z in the MI evolution process. They showed that, in particular, when the amplitude modulation reaches a maximum, the energy in the Fourier components of Eq. (5) is equal to $|f_0|^2 = (\sqrt{2} - 1)^2$ and $|f_n|^2 = 2(\sqrt{2} - 1)^{2n}$. The sideband power geometric series $|f_n|^2$ is compared in Subsection 4.B with our experimental results.

B. Numerical Simulations

The presence of losses and Raman scattering precludes the use of the analytical approaches discussed above for a description of our experimental system, and we thus have to resort to numerical simulations. Indeed, the fiber line in the experimental setup is 2 km long, which makes its linear attenuation nonnegligible. The spontaneous Raman scattering, which causes a power transfer from the pump to a 13.2-THz-shifted Stokes band, may act as an additional source of dissipation. For completeness, Raman scattering between the pump and the sidebands, though it is weak, must also be taken into account in our model.

Moreover, as we detail in Section 4 below, a 99:1 coupler has been inserted into the middle of the propagation fiber, i.e., after 1 km. This coupler allowed us to record the output spectra simultaneously at 1 and 2 km in the fiber line at the expense of a small but nonnegligible insertion loss of 4%. To evaluate the difference between the experimental system and the ideal model of Eqs. (4) we performed numerical simulations of a generalized NLS equation in which we included Raman scattering as well as the distributed losses that are due to linear attenuation and the localized loss of the inserted coupler. We considered realistic coefficients that correspond to the standard telecommunication silica fiber chosen for our experiment, that is, $\beta_2 \approx -21\,\mathrm{ps^2\,km^{-1}}$, $A_{\mathrm{eff}} = 87\,\mu\mathrm{m}^2$, and $\gamma = 1.26\,\mathrm{W^{-1}\,km^{-1}}$ for $n_2 = 3 \times 10^{-20}\,\mathrm{m^2\,W^{-1}}$, where γ takes into account the polarization averaging that is due to residual birefringence, as the propagation fiber was not polarization maintaining.[17] The parameters related to Raman scattering and the losses are detailed in Section 4 below. We calculated η and ϕ numerically from the first three Fourier modes of the numerical solution of the generalized NLS equation. We chose $\Omega = \Omega_{\mathrm{opt}}$ as the initial condition, so the initial MI gain is maximum.

In Fig. 2 we plot (dotted curves) the phase-space portrait associated with the ideal lossless system of Eqs. (4) for $\kappa = -2$ (i.e., for maximum initial MI gain) and the invariant $\alpha = |a_s(\xi = 0)|^2 - |a_a(\xi = 0)|^2 = 0.0023$. These values of κ and α correspond to the input conditions chosen in our experiment for which the parameters were tuned such that $\kappa = -2$, $|a_s(\xi = 0)|^2 = 0.0023$, and $|a_a(\xi = 0)|^2 = 0$; i.e., the small seed signal is set in the Stokes sideband only. Each closed trajectory is the locus of points that represent the values of η and Φ along the

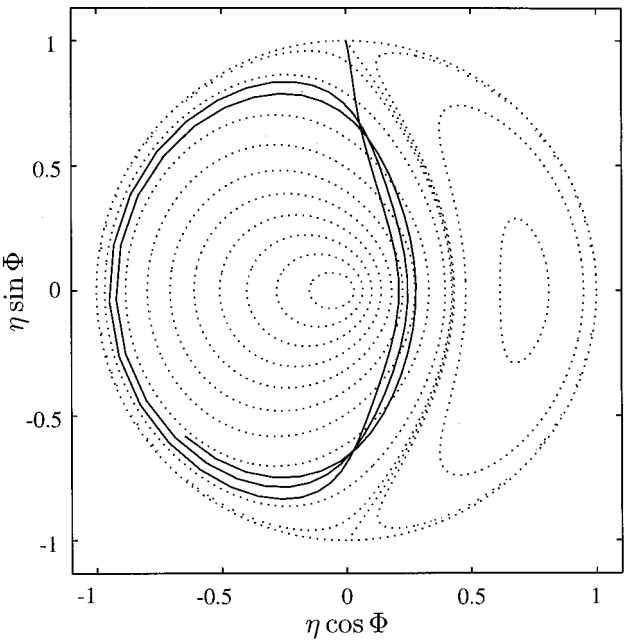

Fig. 2. Phase-space portrait of scalar MI. Dotted curves, trajectories of the ideal lossless system described by Eqs. (4), with $\kappa = -2$ and $\alpha = |a_s(\xi = 0)|^2 - |a_a(\xi = 0)|^2 = 0.0023$. Solid curve, trajectory corresponding to $\kappa = -2$, $|a_s(\xi = 0)|^2 = 0.0023$, and $|a_a(\xi = 0)|^2 = 0$ when losses and Raman scattering are included.

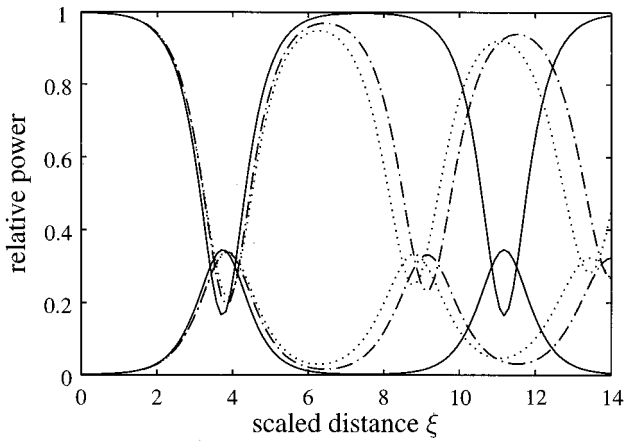

Fig. 3. Evolution of the pump and Stokes powers as a function of ξ. The computed curves were obtained by numerical simulations of the generalized NLS equation. Solid curves, propagation in an ideal lossless fiber; dotted–dashed curves, evolution in a fiber with a linear attenuation of 0.2 dB/km; dotted curves, evolution in the same lossy fiber with the inclusion of the localized 0.2-dB coupler loss and Raman scattering.

fiber for any input condition that satisfies $\alpha = 0.0023$. The phase plane is divided by a separatrix into two regions of periodic orbits that correspond to recurrent nonlinear evolution with a periodic return to the initial conditions. We have superimposed, as solid curves, the trajectory obtained with the generalized NLS equation (including distributed and localized losses, and Raman scattering) for the same initial conditions, $|a_s|^2 = 0.0023$ and $|a_a|^2 = 0$, with $\kappa = -2$.

Figure 3 shows the evolution of the pump and Stokes powers along the scaled distance $\xi = \gamma P_{\text{tot}} z$ as obtained by numerical simulations of the generalized NLS equation. To stress the effect of the distributed loss on the long-term behavior of MI, we compare the evolution in the case of an ideal lossless fiber without Raman scattering (solid curves) with the same evolution when we take only the distributed loss into account (dashed–dotted curves) and when all the losses (linear attenuation and insertion loss of the 99:1 coupler) as well as Raman scattering are included in the model (dotted curves).

As can be seen, distributed losses lead to a speeding up of the MI dynamics, i.e., to a shorter recurrence period. Accordingly, the trajectory for the realistic case represented in Fig. 2 is getting progressively closer to one of the two stable elliptic points. Nevertheless, the pump depletion and the overall evolution remain comparable with those in the reference ideal case of Eqs. (4), at least for the first recurrence period. Regarding Raman scattering, the effect is similar to that of the distributed losses, although it is significantly weaker. The small effect of Raman scattering can be explained by two facts. First, the optimal MI frequency, Ω_{opt}, is much lower than the natural Raman shift. Raman scattering thus has no effect on the power transfer between the waves involved in the MI process, and it consequently induces the same effective loss for the three waves. Second, as the input pump power in the experiment remains far below the threshold for spontaneous Raman scattering, its contribution to MI dynamics, as an effective distributed loss, remains negligible in the evolution depicted in Figs. 2 and 3. As a result, the difference between the long-term evolution of MI with and without inclusion of Raman scattering and coupler loss (shown in Fig. 3 by, respectively, dotted and dotted dashed curves), is essentially due to the insertion loss of the 99:1 coupler. Contrary to what might be thought, the effect of the 0.2-dB localized loss is not equivalent to that of a distributed loss of the same magnitude. The effect of the coupler on the MI evolution depends strongly on the location of the coupler along the fiber line and on the corresponding stage in the MI evolution. For instance, assuming a lossless fiber, a 99:1 coupler inserted after one period of recurrence (i.e., located at $\xi \approx 8$) would have a negligible effect on the further evolution of MI (solid curve). However, when this coupler is inserted about a half period of recurrence ($\xi \approx 4$) as we did in the experiment, its effect on the evolution of the MI is rather comparable to that of distributed loss, leading to an overall evolution similar to that depicted by the dotted–dashed curve in Fig. 3. When both the distributed and the localized losses are taken into account (dotted curve), the ultimate effect is not simply the sum of the two losses; as can be seen, the difference between the dotted and the dotted–dashed curves is slight and can be attributed solely to the coupler loss.

The conclusion of this theoretical analysis is that the perturbative effects of the real experimental system only slightly affect quantitatively, but certainly not qualitatively, the long-term behavior of the MI. In particular, our analysis shows that the perturbations do not prevent the reversible nature of MI from being observed, as no significant change in the dynamics is observed over at least one period of FPU recurrence.

3. SQUARE-SHAPED PULSES

A. Square Pulses versus Gaussian Pulses

The theory presented so far has described the dynamics of MI that has cw waves as initial conditions. However, most experimental studies of MI were performed with pulses instead of cw. Indeed, rigorous observations of MI, which would require high pump power in the cw regime, are hampered by competing nonlinear effects, the stronger of which is Brillouin scattering. This effect causes depletion of the pump power, thus acting as a strong source of dissipation that negates the validity of the predictions drawn from the conservative NLS equation. In experiments with MI, this difficulty is usually overcome by the use of Gaussian-like laser pulses to increase the Brillouin scattering threshold above the pump power by spectral spreading of the pump.[18]

Gaussian pulses much longer than the modulation period of MI are usually considered to operate in the quasi-cw regime.[19] However, whereas Gaussian pulses have proved to be useful in investigation of the initial evolution of MI, they are not suitable for demonstrating its recurrent long-term behavior. The reason is that such pulses contain a continuous range of power levels such that distinct portions of the pulse exhibit different MI gains and frequencies (both the MI gain and frequency reach a maximum at the pulse peak). Each portion of the pulse thus tends to follow its own dynamics but is also connected to the neighboring portions through chromatic

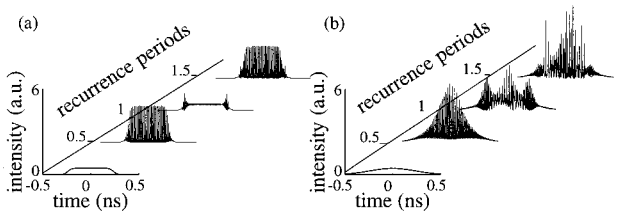

Fig. 4. Envelope evolution over 1.5 recurrence periods of (a) a square pulse and (b) a Gaussian pulse with equal initial peak power (2.3 W) and duration (~550 ps).

dispersion. This pulse behavior leads to a blurring of the modulational pattern and, naturally, the long-term evolution of the pattern strongly diverges from that predicted with cw initial conditions. This result is illustrated in Fig. 4, which shows on the right-hand side the evolution of a Gaussian pulse that undergoes MI in realistic experimental conditions (see below for a detailed description). As can be seen, the blurring of the MI pattern precludes the observation of FPU recurrence. The strong temporal asymmetry is essentially due to the inclusion of Raman scattering in the numerical simulations.

To overcome this pattern blurring, we performed our investigation of MI reversibility by resorting to the use of large square-shaped pulses instead of Gaussian pulses. In doing so we ensured an effective cw regime over the major part of the pulse because the pulse plateau, corresponding to a single power level, is much longer than the pulse rising and trailing edges. Of course, this solution is useful only if the period of the MI pattern is much shorter than the pulse plateau, a condition whose existence we have to ensure in the experiment. In Fig. 4 we compare the evolution of a Gaussian pulse and a square pulse of identical power and full width at half-maximum. These simulations are obtained by numerical solution of the NLS equation [Eq. (1)] with realistic coefficients corresponding to those of the standard telecommunication silica fiber chosen for our experiment (see above). We show the temporal profiles for both pulse types at 0.5, 1, and 1.5 periods of recurrence. As can be seen from these examples, the short rising and trailing edges of the square pulse only slightly perturb the MI dynamics over 1.5 FPU recurrence periods over which MI reversibility is clearly visible, contrary to what happens with the Gaussian pulse.

Nevertheless, we may expect some differences between the long-term behavior of a square-shaped pulse and that of a pure cw. The sharp rising and trailing edges, in particular, give rise to dispersive waves as they propagate along the fiber. In this way, these edges act as an additional dissipation source in the system that significantly affects the long-term behavior of MI. This behavior is well illustrated in Fig. 5, where we plot the evolution of the pump and the Stokes powers as functions of ξ for a pure cw (solid curve) and a square pulse (dashed curve) that correspond to those generated in the experiment (see below). We notice that the pump and sideband powers of a square pulse decrease much faster than for a cw pump. However, the qualitative features that denote the reversibility of the MI process—the recurrence distance in particular—are basically the same in both cases, at least for the first few periods. As a consequence, this brief analysis proves that the use of sufficiently large square pulses is appropriate for demonstrating the reversibility of MI.

B. Square-Pulse Generator

The design of a square-pulse generator has therefore been crucial in producing MI reversibility in optical fibers. This source was conceived and realized experimentally with a nonlinear optical loop mirror (NOLM).[20] The NOLM is an all-fiber antiresonant Sagnac interferometer. It consists of a fiber loop closed by the two output ports of a balanced (insertion loss, 3 dB) fiber coupler. When a signal enters the input port, its energy is split through the coupler into two signals of equal intensity. The clockwise and counterclockwise propagating signals accumulate the same phase during propagation and interfere destructively at the output port. The input optical energy is therefore entirely reflected back to the input port of the device, acting then as a mirror.

Partial transmission through the NOLM output port can, however, be obtained if the symmetry between the clockwise and the counterclockwise optical paths in the loop is broken. To generate square pulses, we operate the NOLM in a two-wavelength configuration.[21] The switching of a square-shaped portion of a cw signal at one wavelength is achieved by injection into one direction of the loop (say, the clockwise direction) an intense control pulse at a different wavelength, as can easily be understood from Fig. 6. A low-power cw signal (~8 mW) is provided by a distributed-feedback laser tuned to 1551 nm, and the high-power control pulse is provided by a mode-locked Nd:YAG laser emitting 120-ps pulses at 1064 nm at a repetition rate of 82 MHz. The control pulse is injected into the loop through coupler WDM1 (Fig. 6) located close to the 50:50 coupler. It propagates clockwise and gets out of the loop at coupler WDM2. The loop is made from a 360-m-long standard single-mode fiber. As the fiber is not polarization maintaining, a polarization controller (PC) has been inserted into the loop to ensure correct operation of the device. Both clockwise and counterclockwise signal waves experience cross-phase modula-

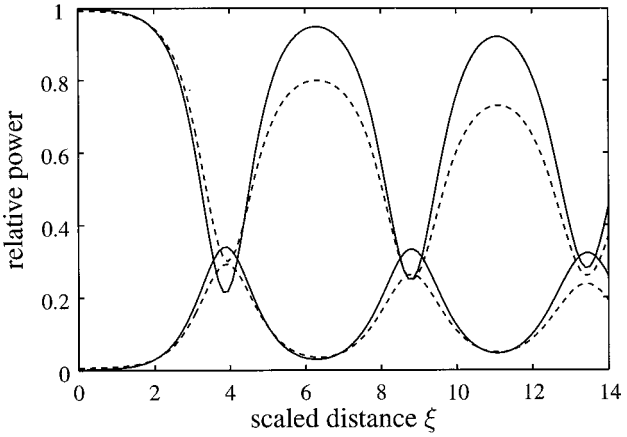

Fig. 5. Evolution of the pump and Stokes powers versus ξ for $\kappa = -2$ and $|a_s|^2 = 0.0023$ when linear attenuation, insertion loss of the 99:1 coupler, and Raman scattering have been taken into account. Input waves are a cw (solid curves) and a square pulse (dashed curves).

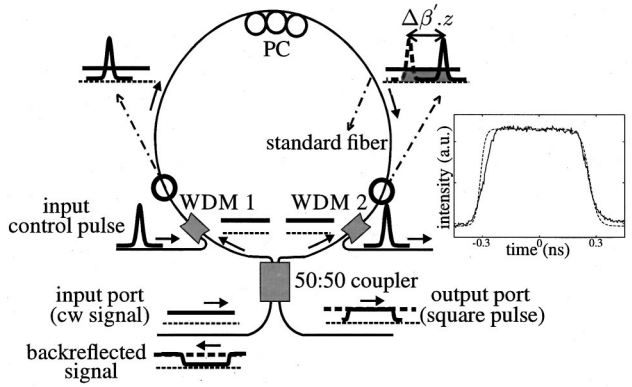

Fig. 6. Experimental setup of the square-pulse generator. Inset, measured output square-pulse profile (solid curve) and profile obtained after deconvolution (dashed curve).

tion induced by the control pulse. It has been shown[22] that the phase changes in the clockwise, Φ_{clkw}, and the counterclockwise, Φ_{cntw}, cw signals caused by a control pulse $P_c(t)$ can be written, respectively, as

$$\Phi_{\mathrm{clkw}}(t) \doteq 2\int_0^L P_c(t - \Delta\beta' z)\mathrm{d}z, \tag{6a}$$

$$\Phi_{\mathrm{cntw}} \doteq 2\langle P_c\rangle L, \tag{6b}$$

where L is the loop length, $\langle P_c\rangle$ is the time-averaged power of the control beam, and $\Delta\beta' = 1/v_{\mathrm{gc}} - 1/v_{\mathrm{gs}}$ is the difference in group delay between the control and the signal waves. The walk-off between the clockwise signal and the control pulse was evaluated through group-delay measurements and was found to be -1.5 ps/m. Owing to this walk-off, a phase shift Φ_{clkw} is imparted over a portion, of duration $\Delta\beta' L$, of the clockwise signal. The intensity transmission of the NOLM is

$$T_I(t) = \sin^2\left[\frac{\Delta\Phi(t)}{2}\right], \tag{7}$$

where $\Delta\Phi(t) = \Phi_{\mathrm{clkw}}(t) - \Phi_{\mathrm{cntw}}$. The loop length L is 360 m and yields a walk-off time of $\sim \Delta\beta' L = 540$ ps in the standard silica fiber that constitutes the loop. This time represents the duration of the signal transmitted by the NOLM. The best contrast in transmitted intensity at the output of the NOLM is obtained when nonlinear phase difference $\Delta\Phi$ amounts to π. We verified experimentally that this condition is obtained when the peak power of the control pulses is tuned to 17 W. Note that $\Phi_{\mathrm{cntw}} \approx 0$, because the average control power in the counterclockwise optical path is as low as $\sim$175 mW. The transmitted square pulses were measured with a fast photodiode (response time, $\sim$70 ps) and displayed on a sampling oscilloscope. The inset of Fig. 6 shows the measured square-pulse profile as well as the profile obtained after deconvolution with the impulse response of the detection system.

4. EXPERIMENT

A. Experimental Setup

Figure 7 shows the experimental setup. The square-shaped pulses generated by the NOLM at 1551 nm constituted the pump wave. MI was seeded by a small cw signal emitted by a wavelength-tunable source (external-cavity semiconductor laser). The seed and the pump wave were amplified through an erbium-doped fiber amplifier (preceded by a preamplifier with a saturated output power of 18 mW), pumped by four wavelength-multiplexed semiconductor lasers. The pump and seed waves were then injected into a 2.070-m-long low-loss (0.2 dB/km) single-mode standard telecommunication fiber whose parameters were as given above in Subsection 2.B. A 99:1 coupler (insertion loss, 0.2 dB) was inserted after a fiber length of 1 km such that the output spectra could be recorded simultaneously at the end and at the middle of the fiber line. These measurements were performed with an optical spectrum analyzer.

After amplification, the plateau power of the pump pulses could be tuned from 1 to 2.3 W at the input of the fiber line, whereas the cw seed power was always maintained $\sim$27 dB lower. The power threshold for Raman scattering is[23] $P_0^{\mathrm{th}} \simeq 16A_{\mathrm{eff}}/(g_R L_{\mathrm{eff}})$, where $g_R \simeq 10^{-13}\,\mathrm{mW}^{-1}$ is the Raman-gain coefficient, $L_{\mathrm{eff}} \simeq 2\,\mathrm{km}$ is the effective interaction length, and $A_{\mathrm{eff}} = 87\,\mu\mathrm{m}^2$ is the effective core area. We can thus find that $P_0^{\mathrm{th}} \simeq 7$ W, which is well above the maximum pump power (2.3 W) that we reached in the experiment. Consequently, the spontaneous Raman gain remained negligible throughout the experiment and did not affect the MI evolution in the fiber, as stated above in Subsection 2.B. Furthermore, as the mean duration of the square pulses ($\sim$550 ps) was much smaller than the acoustic phonon lifetime ($T_B = 16$ ns) involved in the Brillouin scattering process, it can be shown (see, e.g., Chap. 9 of Ref. 23) that the Brillouin gain is reduced below the Raman gain and is therefore completely eliminated.

The seed frequency was tuned to maintain detuning frequency Ω at its maximum MI gain value, Ω_{opt}, for all pump power levels, which corresponds to a tuning range of 340–520 GHz (0.44–0.66 nm in wavelength), as we ensured in practice by adjusting, for each input pump power, the seed frequency to the frequency of the maximum of the Stokes sideband that appeared in the spontaneous MI regime. This sideband, which reproduces the MI spectral gain profile, is directly visible (i.e., distinguishable from noise) on the optical spectrum analyzer, provided that the pump power is greater than 1 W. For lower pump power, the spontaneous MI gain is so weak that the maximum cannot be isolated from the noise background, which explains the lower pump power limit of 1 W that we had to respect in our experiment.

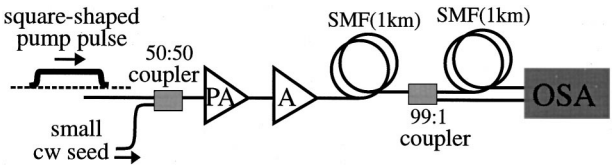

Fig. 7. Experimental setup: PA, preamplifier with an output power of $\sim$18 mW; A, Er^{3+}-doped fiber amplifier, 25 m long, pumped by four wavelength-multiplexed laser diodes near 980 nm; SMFs, standard telecommunication single-mode fibers; OSA, optical spectrum analyzer.

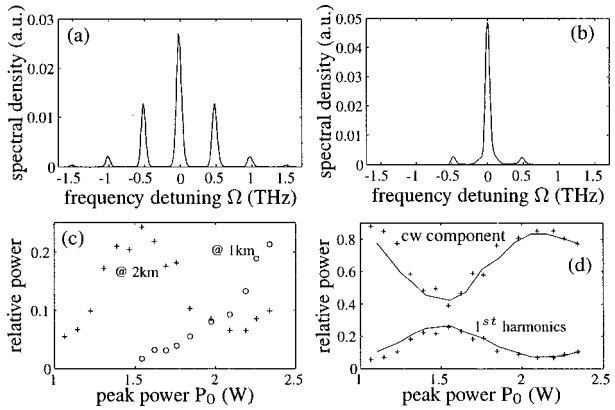

Fig. 8. Square-pulse spectra on a linear scale measured at (a) 1 km and (b) 2 km at a pump power of $P_0 = 2.2\,\mathrm{W}$. (c) Relative power of the first sideband, P_1/P_0, versus P_0 at 1 and 2 km. (d) Experimental (crosses) and calculated (solid curves) relative sideband and pump powers versus P_0 at 2 km.

B. Experimental Results

The spectra at 1 and 2 km were recorded under the conditions described above for several values of input power P_0. As can be seen from Figs. 8(a) and 8(b), which show the measured spectra at 1 and 2 km for $P_0 = 2.2\,\mathrm{W}$, the spectrum exhibits weak sidebands at 2 km, whereas significantly stronger sidebands were observed at 1 km. This result is in itself a good indication of the reversibility of the MI process.

Figure 8(c) shows the evolution of the relative power of the first sideband P_1/P_0, as a function of the pump power P_0 at 1 and 2. We verify that the relative sideband power at 2 km initially grows with P_0 to reach a maximum at $P_0 \simeq 1.5\,\mathrm{W}$ and then decreases to a minimum located at $P_0 \simeq 2.2\,\mathrm{W}$ before increasing again. It is approximately when the sideband power at 2 km reaches its maximum that we can start the measurement of the sideband power at 1 km because it becomes distinguishable from noise only at the corresponding pump power, $P_0 \simeq 1.5\,\mathrm{W}$. A further increase of pump power leads to an increase in the sideband power at 1 km and to a decrease in the sideband power at 2 km. This measurement clearly demonstrates the reversibility of MI. Figure 8(d) shows the evolution both of the relative powers of the cw component P_{cw}/P_0 and of the first sideband P_1/P_0 at 2 km. As can be seen, the maximum of sideband power observed at $P_0 = 1.55\,\mathrm{W}$ corresponds to a minimum of cw component power, in agreement with theory. In Fig. 8(d) we also show the theoretical (solid) curves obtained by numerical simulation of the generalized NLS equation (including all losses and Raman scattering). Excellent agreement between theory and experiment is verified, but it should be noted that, to obtain this agreement, we had to perform our simulation with square pulses. Although the use of square pulses ensures a quasi-cw regime of good spectral quality, the rising and trailing edges have a significant effect on MI, as discussed in Section 3. This explains why, contrary to what was predicted with the lossless NLS, Eq. (1), the minimum of sideband power at 2 km does not coincide precisely with the maximum at 1 km in Fig. 8(c).

However, before further studying the reversibility of MI, let us now analyze Fig. 9, which shows the MI spectrum on a logarithmic scale obtained at maximum pump depletion at 1 km, corresponding to a pump power of $P_0 = 2.35\,\mathrm{W}$. One can verify from this figure that the power in the spectral sidebands follows a geometric progression law. Our analysis indicates that the power in the Stokes and anti-Stokes sidebands and their higher-order harmonics is distributed according to a geometric progression (i.e., the logarithm of successive sideband powers exhibits a linear decay law) of mean ratio ~ 0.175, with standard deviations of $\sim 15\%$ for the Stokes modes and $\sim 5\%$ for the anti-Stokes modes. This result is in remarkably good agreement with Akhmediev's theory (Subsection 2.A), which predicts a ratio of $(\sqrt{2}-1)^2 \simeq 0.17$ when the amplitude modulation of the input cw and the pump depletion reach a maximum.

To make a more-detailed experimental investigation of the long-term behavior of MI, we observed the evolution of the output spectrum for a fixed fiber length with various input pump power conditions. This procedure does not correspond to that considered in the theoretical section, Section 2 above, where the dynamics of MI were studied with respect to the propagation distance. Our experimental results can, however, be represented by the scaled propagation distance $\xi = \gamma P_{\mathrm{tot}} D$ that we introduced in Eqs. (4). One can indeed study the evolution in ξ at a fixed value of z by simply varying input power P_0. With $z = 2$ km, the range 1–2.3 W of the input power corresponds to a variation of ξ from 2.77 to 6.10, which allows, as we shall see, for a comfortable and detailed study of the reversibility of MI. Note, however, that variable ξ is not strictly equivalent to the physical propagation distance in our experiment because it does not allow one to take into account the effect of coupler insertion loss, whose value and position vary as functions of the input pump power.

The reversibility of MI is once again clearly demonstrated by the experimental results shown in Fig. 10. Figures 10(a) and 10(b) show the evolution of the MI spectrum in the form of a density plot on a logarithmic power scale and as a surface plot on a linear power scale, respectively [exact scaled units are used on the two other axes, $\xi = \gamma P_0 z$ and $\omega = (\gamma P_0/|\beta_2|)^{-1/2}\Omega$]. We observe that the energy, initially confined mainly to the pump wave, is progressively transferred to the sidebands and their higher harmonics, which leads to a strong pump depletion of approximately 70%, as predicted theoretically in Ref.

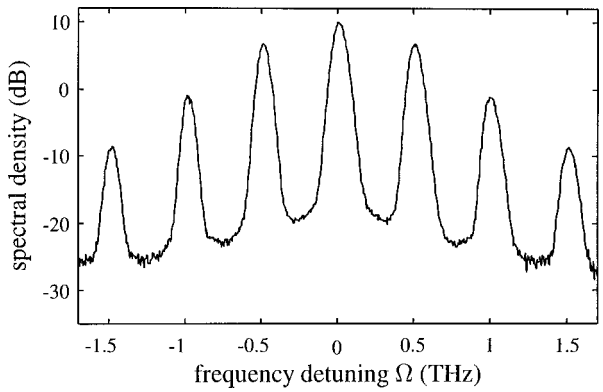

Fig. 9. Square-pulse spectrum on a logarithmic scale at an input pump power $P_0 = 2.35\,\mathrm{W}$ after 1 km.

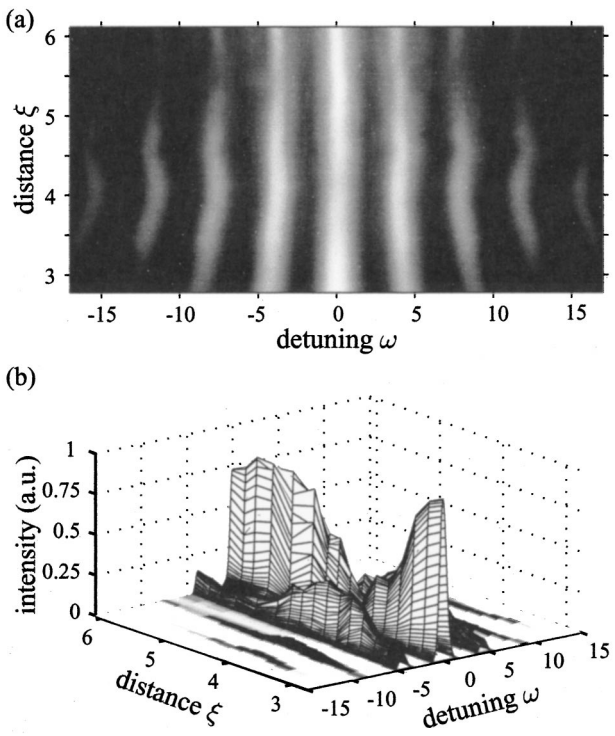

Fig. 10. Evolution of the recorded MI spectrum as a function of scaled longitudinal variable $\xi = \gamma P_0 z$: (a) log scale, (b) linear scale.

10. As many as eight detectable modes are involved in this energy exchange process. After a certain propagation distance ($\xi = 4.1$) the energy transfer is reversed, and all the power flows back from the sideband modes to the pump wave. This reciprocal energy exchange process between the pump and a significant number of sideband modes is nothing but the spectral signature of the FPU recurrence phenomenon.[5] The remarkable feature of Fig. 10 is that it shows that the power transfer between the sideband modes is perfectly synchronous despite the relatively large number of modes involved. As stated theoretically by Yuen and Ferguson,[4] it is this synchronism that accounts for a (nearly complete) return to the initial condition.

5. CONCLUSIONS

In this paper we have presented what we believe is the first clear-cut experimental evidence of the reversibility of modulational instability in optical fibers. Although this feature of MI in systems ruled by the NLS equation has been predicted for years in numerous and extensive theoretical studies in various physical contexts, to our knowledge it had never been observed in a laboratory experiment with optical waves. The only experimental proof of this reversibility was given 24 years ago in an old study of deep-water waves that are also ruled by the NLS equation.[3]

Our experimental results, shown in Figs. 8(c) and 8(d), definitely demonstrate that MI in fibers in reversible and exhibits the FPU recurrence. This demonstration is reinforced in Fig. 10, in which we can observe the synchronous evolution of as many as eight sidebands. By showing that the NLS equation is an adequate model for describing the long-term behavior of MI in fibers, our results provide further proof of the validity of the NLS equation for the description of complex nonlinear dynamic processes in optical fibers, an issue that is still often the subject of debate. The most striking result that corroborates this conclusion is the quantitative verification of the geometric progression of the higher-order sideband powers predicted by Akhmediev and Korneev.[12]

From the application point of view, some authors have suggested exploitating the reversibility of MI for switching purposes.[10,24] An all-optical switch based on long-term MI dynamics must be operated in a range of parameters where $-1 < \kappa < 0$ so, the output pump (or sideband) power strongly depends on the initial relative phase $\Phi(\xi = 0)$, yielding either a periodic power exchange between the waves or aperiodic pump depletion, which leads asymptotically to $\eta = 0$ according to the launching conditions. However, in the case of scalar MI considered here, the truncated three-wave model used to describe such dynamics is no longer valid for $-1 < \kappa < 0$ because higher-order sideband harmonics fall inside the MI gain band and therefore can not be neglected. However, considering the quality of the results presented here, one can reasonably expect that the experimental study of the long-term dynamics of polarization MI in weakly birefringent fibers for which narrow gain bands have been predicted[25] and observed[26] will lead to potential applications to all-optical switching. Such studies will be the object of our future investigations.

ACKNOWLEDGMENTS

This research was carried out under grant P4-07 of the Inter-University Attraction Pole program of the Belgian government. The research of G. Van Simaeys is supported by the Fonds pour la Formation à la Recherche dans l'Industrie et l'Agriculture, and that of M. Haelterman by the Fonds National de la Recherche Scientifique (Belgium). G. Van Simaeys acknowledges helpful technical assistance from S. Coen.

G. Van Simaeys's e-mail address is gvsimaey@ulelb.ac.be.

REFERENCES

1. T. B. Benjamin and J. E. Feir, "The disintegration of wave trains on deep water. 1. Theory," J. Fluid Mech. **27**, 417–430 (1967).
2. T. B. Benjamin, "Instability of periodic wavetrains in nonlinear dispersive systems," Proc. R. Soc. London Ser. A **299**, 59–75 (1967).
3. B. M. Lake, H. C. Yuen, H. Rungaldier, and W. E. Ferguson, "Nonlinear deep-water waves: theory and experiment. 2. Evolution of a continuous wave train," J. Fluid Mech. **83**, 49–74 (1977).
4. H. C. Yuen, J. Warren, and E. Ferguson, "Relationship between Benjamin–Feir instability and recurrence in the nonlinear Schrödinger equation," Phys. Fluids **21**, 1275–1278 (1978).
5. E. Fermi, J. Pasta, and H. C. Ulam, "Studies of nonlinear problems," in *Collected Papers of Enrico Fermi*, E. Segrè, ed. (U. Chicago Press, Chicago, Ill., 1965), Vol. 2, pp. 977–988.

6. T. Taniuti and H. Washimi, "Self-trapping and instability of hydromagnetic waves along the magnetic field in a cold plasma," Phys. Rev. Lett. **21**, 209–212 (1968).
7. F. D. Tappert and C. N. Judice, "Recurrence of nonlinear ion acousitc waves," Phys. Rev. Lett. **29**, 1308–1311 (1972).
8. P. Henrotay, "Periodic solutions and recurrence for nonlinear Schrödinger equation: a Fourier-mode approach," J. Mec. **20**, 159–168 (1981).
9. E. Infeld, "Quantitive theory of the Fermi–Pasta–Ulam recurrence in the nonlinear Schrödinger equation," Phys. Rev. Lett. **47**, 717–718 (1981).
10. G. Cappellini and S. Trillo, "Third-order three-wave mixing in single-mode fibers: exact solutions and spatial instability effects," J. Opt. Soc. Am. B **8**, 824–838 (1991).
11. R. H. Stolen and J. E. Bjorkholm, "Parametric amplification and frequency conversion in optical fibers," IEEE J. Quantum Electron. **QE-18**, 1062–1072 (1982).
12. N. N. Akhmediev and V. I. Korneev, "Modulation instability and periodic solutions of the nonlinear Schrödinger equation," Theor. Math. Phys. **69**, 1089–1093 (1986) [Teor. Mat. Fiz. **69**, 189–194 (1986)].
13. N. N. Akhmediev, V. M. Eleonskii, and N. E. Kulagin, "Exact first-order solutions of the nonlinear Schödinger equation," Theor. Math. Phys. **72**, 809–818 (1987) [Teor. Mat. Fiz. **72**, 183–196 (1987)].
14. S. G. Murdoch, R. Leonhardt, and J. D. Harvey, "Nonlinear dynamics of polarization-modulation instability in optical fiber," J. Opt. Soc. Am. B **14**, 3403–3411 (1997).
15. S. Trillo and S. Wabnitz, "Dynamics of the nonlinear modulation instability in optical fibers," Opt. Lett. **16**, 986–988 (1991).
16. M. Haelterman and A. P. Sheppard, "Vector soliton associated with polarization modulational instability in the normal dispersion regime," Phys. Rev. E **49**, 3389–3399 (1994).
17. S. G. Evangelides, L. F. Mollenauer, J. P. Gordon, and N. S. Bergano, "Polarization multiplexing with solitons," J. Lightwave Technol. **10**, 28–35 (1992).
18. D. Cotter, "Suppression of stimulated Brillouin scattering during transmission of high-power narrowband laser light in monomode fibre," Electron. Lett. **18**, 638–640 (1982).
19. K. Tai, A. Hasegawa, and A. Tomita, "Observation of modulational instability in optical fibers," Phys. Rev. Lett. **56**, 135–138 (1986).
20. N. Doran and D. Wood, "Nonlinear-optical loop mirror," Opt. Lett. **13**, 56–58 (1988).
21. K. J. Blow, N. J. Doran, B. K. Nayar, and B. Nelson, "Two-wavelength operation of the nonlinear fiber loop mirror," Opt. Lett. **15**, 248–250 (1990).
22. M. Jinno and T. Matsumoto, "Nonlinear Sagnac interferometer switch and its applications," IEEE J. Quantum Electron. **28**, 875–882 (1992).
23. G. P. Agrawal, *Nonlinear Fiber Optics*, 2nd ed. (Academic, San Diego, Calif., 1995).
24. G. Cappellini and S. Trillo, "Energy conversion in degenerate four-photon mixing in birefringent fibers," Opt. Lett. **16**, 895–897 (1991).
25. S. Wabnitz, "Modulational polarization instability of light in a nonlinear birefringent dispersive medium," Phys. Rev. A **38**, 2018–2021 (1988).
26. S. G. Murdoch, R. Leonhardt, and J. D. Harvey, "Polarization modulation instability in weakly birefringent fibers," Opt. Lett. **20**, 866–868 (1995).